

Magnetic Dipole Portal Vector Dark Matter at Fixed-Targets

Avik Banerjee,^a Riccardo Catena,^b and Taylor R. Gray^b

^a*Department of Theoretical Physics, Tata Institute of Fundamental Research, Homi Bhabha Road, Mumbai 400005, India*

^b*Chalmers University of Technology, Department of Physics, SE-412 96 Göteborg, Sweden*

E-mail: avik.banerjee.205@tifr.res.in, catena@chalmers.se,
taylor.gray@chalmers.se

ABSTRACT: We present a model featuring a sub-GeV vector dark matter by augmenting the Standard Model with a new non-Abelian dark $SU(2)_D$, spontaneously broken by the vacuum expectation values of a scalar doublet and a triplet. Interactions between the dark and visible sectors arise through a dimension-5 non-Abelian *avatar* of kinetic mixing portal, inducing effective magnetic dipole couplings of the dark matter, with the photon and Z boson. The resulting spectrum of the dark gauge bosons naturally exhibits an inverse mass hierarchy between the dark matter and the Z' , leading to interesting phenomenology at fixed target experiments such as LDMX through dark off-shell bremsstrahlung, dark Higgsstrahlung, invisible vector meson decay, and visible decays. We compute the thermal relic abundance across sub-GeV dark matter masses, with regions of freeze-out proceeding via forbidden annihilation into dark sector states or direct annihilation into Standard Model states. Bounds from a broad set of laboratory probes, along with cosmological and astrophysical observations, are incorporated in our analysis. Among them, the most restrictive bounds originate from direct detection experiments, Big Bang Nucleosynthesis, collider searches, and the CMB. Our results demonstrate that a sizeable region of the parameter space remains consistent with the observed relic abundance and the existing experimental results.

Contents

1	Introduction	1
2	The Model	3
3	Freeze-out Relic Density	5
3.1	Thermalization Condition	6
4	Current Experimental Bounds	7
4.1	Colliders	7
4.2	Direct Detection	7
4.3	Electroweak Precision Measurements	8
4.4	Astrophysical and Cosmological Constraints	9
5	Sensitivity at Fixed-Target Experiments	10
5.1	Dark Bremsstrahlung	11
5.2	Dark Higgs-strahlung	12
5.3	Invisible Vector Meson Decay	13
5.4	Visible Searches	14
6	Relic Targets, Constraints, and LDMX Projections	15
7	Conclusion	16
A	Invisible Vector Meson Decay Rate	17

1 Introduction

The quest to uncover the elusive nature of dark matter (DM), strongly supported by evidence across a wide range of cosmological and astrophysical observations [1], continues along several complementary experimental and theoretical directions. Major global efforts are underway to: (i) perform *direct detection* searches aiming to observe interactions of the Galactic DM at the terrestrial detectors; (ii) infer DM properties through its imprint on *cosmological* observables such as the cosmic microwave background (CMB); (iii) identify possible *astrophysical* signals of DM annihilation or decay into Standard Model (SM) particles via *indirect detection* probes; (iv) constrain DM interactions and their effects on the SM through *high-precision measurements* of the SM parameters; and (v) explore the production of DM and dark-sector states in *collider* experiments.

Along many of these fronts, the weakly interacting massive particle (WIMP) [2, 3] has long served as the leading dark matter (DM) candidate, primarily due to its ability to naturally reproduce the observed relic abundance through weak-scale interactions. Although the WIMP paradigm remains appealing, growing attention has turned toward alternative possibilities. In particular, a broad class of models now considers DM candidates with masses below the GeV scale. Such light DM scenarios require the presence of a new mediator particle to facilitate interactions between the DM and the SM, thereby avoiding the Lee–Weinberg bound—an upper mass limit for thermal relics with weak-scale couplings [4].

Since sub-GeV DM is too light to produce detectable nuclear recoils in conventional direct detection experiments, novel search strategies have been developed. A prominent approach involves direct detection of DM–electron scattering in target materials [5, 6], which provides optimal sensitivity to light DM. Concurrently, accelerator-based experiments offer complementary avenues to probe light DM, either through missing energy or momentum signatures, direct DM scattering in downstream detectors, or via visible decays of the mediator into SM particles [7, 8]. Several current and upcoming experiments are specifically designed to explore this light DM regime [9].

Fixed-target experiments are particularly well suited for probing light dark matter (DM) owing to their well-characterized backgrounds, high luminosities, and favorable forward kinematics [10]. The forthcoming *Light Dark Matter eXperiment (LDMX)*—a missing-momentum experiment with a planned 8 GeV electron beam incident on a tungsten target—is projected to substantially extend the current sensitivity reach [11]. Theoretical studies relevant to LDMX and similar light DM searches have predominantly focused on simplified models featuring a dark photon mediator (A') [12] as well as spin-1 DM scenarios encompassing both simplified and extended frameworks [13]. More recently, dark photon models incorporating higher-order dark electromagnetic moments have also been explored [14].

In general, any heavy new particle that can be produced in electron–nuclear collisions, such as through dark bremsstrahlung, and subsequently escape detection due to its feeble interactions with the SM, constitutes a viable target for LDMX. This broad experimental reach renders LDMX a promising platform to explore a diverse landscape of theoretical possibilities within the dark sector. Among the many possibilities, spin-1 (vector) dark matter (DM) [15–23] has been explored in diverse contexts, ranging from direct detection phenomenology [24–26] to gravitational-wave signatures [27, 28] and freeze-in production mechanisms [29]. Previous studies, such as Ref. [13], have focused on the on-shell production of spin-1 DM at fixed-target facilities like LDMX.

The present work examines a spin-1 DM scenario featuring a complementary region of parameter space in which the mass hierarchy between the mediator and DM is reversed, i.e. $m_{Z'} < 2m_{\text{DM}}$. In this regime, the mediator is kinematically forbidden from decaying invisibly into DM pairs. Consequently, DM production proceeds via an off-shell mediator, leading to a suppressed rate compared to the conventional on-shell scenario. Meanwhile, the mediator predominantly decays into visible final states, offering distinctive signatures for experimental searches in the visible sector.

Motivated by this complementary and relatively unexplored phenomenology, we propose a theoretical framework for a light spin-1 dark matter (DM) candidate. In this construction, the SM gauge group is extended by a new non-Abelian gauge symmetry, $SU(2)_D$ ¹, which breaks spontaneously via the vacuum expectation values (vevs) of two scalar fields charged under the $SU(2)_D$: a triplet, Σ_D , and a doublet, Φ_D . The corresponding massive gauge bosons form a triplet, comprising the DM particle X_μ^\pm , and the mediator Z'_μ . We note that the model we present is complementary to the recent work [30], where a vector DM scenario with similarities is considered.

To connect the dark and visible sectors, we introduce a novel dimension-5 portal operator that embodies a non-Abelian *avatar* of kinetic mixing, that mediates interactions between the DM, the Z' , and the SM photon and Z boson. This framework naturally realizes an inverse mass hierarchy between the Z' and the DM, generates momentum-suppressed DM-photon interactions through an effective magnetic dipole operator, and induces additional couplings of the dark scalar fields with the SM. Together, these features open new invisible production channels that can be probed at LDMX and other fixed-target experiments.

Building on the theoretical framework outlined in Section 2, we explore the phenomenology of the model in the sub-GeV mass range, considering constraints and signatures across various experimental frontiers. The DM relic abundance is computed under the assumption of thermal freeze-out, as discussed in Section 3. In Section 4, we examine existing constraints on the model parameter space arising from the collider searches, electroweak precision tests, cosmological observations, and astrophysical probes. The projected sensitivities of fixed-target experiments, with particular emphasis on LDMX [11] and NA64 [31], are discussed in Section 5. In Section 6, all relevant constraints are placed alongside thermal targets, revealing the complementarity of all bounds and the parameter regions yet to be excluded, followed by concluding remarks in Section 7.

2 The Model

We augment the SM gauge group by a new non-Abelian dark gauge symmetry,

$$SU(2)_L \otimes U(1)_Y \otimes SU(2)_D, \quad (2.1)$$

which contains a scalar doublet (Φ_D) and a scalar triplet (Σ_D) charged under the $SU(2)_D$. The field content of the dark sector is summarized in Table 1. The Lagrangian of the dark sector is given by

$$\mathcal{L}_{\text{DM}} = -\frac{1}{4}X_{\mu\nu}^a X^{a\mu\nu} + |D_\mu \Phi_D|^2 + |D_\mu \Sigma_D|^2 - V(\Phi_D, \Sigma_D), \quad (2.2)$$

¹In contrast to previous studies that introduce an additional $SU(2) \times U(1)$ gauge structure [16, 21], the present framework contains no extra $U(1)$ factor.

Fields	Spin	$SU(2)_D$	Symbols	$U(1)_D$
Φ_D	0	2	$\Phi_D = \begin{pmatrix} \phi_D^+ \\ \frac{\phi_D^0 + i\chi^0}{\sqrt{2}} \end{pmatrix}$	$\phi_D^\pm : \pm 1/2$
Σ_D	0	3	$\Sigma_D = \frac{1}{2} \begin{pmatrix} \Sigma_D^0 & \sqrt{2}\Sigma_D^+ \\ \sqrt{2}\Sigma_D^- & -\Sigma_D^0 \end{pmatrix}$	$\Sigma_D^\pm : \pm 1$
X_μ^a	1	3	$X_\mu^a = \begin{pmatrix} X_\mu^+ \\ X_\mu^- \\ X_\mu^0 \end{pmatrix}, X_\mu^\pm = \frac{1}{\sqrt{2}}(X_\mu^1 \mp X_\mu^2)$	$X_\mu^\pm : \pm 1$

Table 1: Particle content and quantum numbers of the dark sector fields.

where the covariant derivatives are $D_\mu \Phi_D = \partial_\mu \Phi_D - i\frac{g_D}{2}\tau^a X_\mu^a \Phi_D$, and $D_\mu \Sigma_D = \partial_\mu \Sigma_D - i\frac{g_D}{2}[\tau^a, \Sigma_D]X_\mu^a$, and the scalar potential reads

$$V(\Phi_D, \Sigma_D) = -\mu_{\Phi_D}^2 \Phi_D^\dagger \Phi_D - \mu_{\Sigma_D}^2 \text{Tr}[\Sigma_D^2] + \mu_{\Phi_D \Sigma_D} \Phi_D^\dagger \Sigma_D \Phi_D + \lambda_{\Phi_D} (\Phi_D^\dagger \Phi_D)^2 + \lambda_{\Sigma_D} \text{Tr}[\Sigma_D^2]^2 + \lambda_{\Phi_D \Sigma_D} \Phi_D^\dagger \Phi_D \text{Tr}[\Sigma_D^2]. \quad (2.3)$$

The $SU(2)_D$ symmetry is spontaneously broken when the triplet and doublet scalars acquire vevs,

$$\langle \Sigma_D \rangle = \frac{v_\Sigma}{2} \begin{pmatrix} 1 & 0 \\ 0 & -1 \end{pmatrix}, \quad \langle \Phi_D \rangle = \frac{1}{\sqrt{2}} \begin{pmatrix} 0 \\ v_\Phi \end{pmatrix}. \quad (2.4)$$

After spontaneous breaking of the dark gauge symmetry, the masses of the dark vector bosons are obtained as

$$m_{X^\pm}^2 = \frac{g_D^2 v_D^2}{4}, \quad m_{X^0}^2 = \frac{g_D^2 v_D^2}{4} \sin^2 \beta, \quad (2.5)$$

where we define

$$v_D \equiv \sqrt{v_\Phi^2 + 2v_\Sigma^2}, \quad \text{and} \quad \tan \beta \equiv \frac{v_\Phi}{\sqrt{2}v_\Sigma}. \quad (2.6)$$

The triplet vev contributes solely to the masses of X_μ^\pm , while the doublet vev generates masses for both X_μ^\pm and X_μ^0 . This distinction arises because X_μ^\pm carry charge under a global $U(1)_D$ symmetry associated with the τ^3 generator of $SU(2)_D$. The doublet vev spontaneously breaks this $U(1)_D$, leaving behind a residual discrete \mathbb{Z}_2 symmetry that acts as a stabilizing symmetry for the dark matter. The $U(1)_D$ charges of the fields are summarized in the last column of Table 1. We identify the dark-charged gauge bosons X_μ^\pm as the lightest states carrying nontrivial \mathbb{Z}_2 charge, and therefore as the stable dark matter candidates in this framework. It is worth noting that this framework naturally realizes an inverse mass hierarchy between the dark matter and the neutral gauge boson X_μ^0 , a distinctive feature that gives rise to interesting phenomenological consequences, as elaborated in the subsequent sections.

The physical scalar spectrum involves a dark-charged scalar and two neutral scalars. Notably, we neglect the Higgs portal interaction terms in the scalar potential, since the thermal freeze-out of dark matter via Higgs portal receives stringent bounds from multiple observables, such as Higgs invisible decays, modifications to the triple-Higgs coupling, and di-Higgs production channels [32–34].

Here instead, we propose a novel interaction between the dark and visible sectors arising from a dimension-5 non-Abelian gauge kinetic portal operator,

$$\mathcal{L}_{\text{int}} = -\frac{\sin \zeta}{2v_\Sigma} \text{Tr} [\Sigma_D X_{\mu\nu}] B^{\mu\nu}, \quad (2.7)$$

where $X_{\mu\nu} \equiv \sigma^a X_{\mu\nu}^a$, and $B_{\mu\nu}$ is the hypercharge field strength tensor and ζ parametrizes the strength of the interaction, adapting the notation from [16]. When Σ_D receives vev, a kinetic mixing between the X_μ^0 and the hypercharge gauge boson is generated as

$$\mathcal{L}_{\text{mix}} = -\frac{\sin \zeta}{2} X_\mu^0 B^{\mu\nu}, \quad (2.8)$$

which leads to the mixing of X_μ^0 with the SM neutral gauge bosons. We label the resulting BSM mass eigenstate as Z' . In addition to the kinetic mixing, \mathcal{L}_{int} induces contact interactions of the DM with the Z boson and photon via magnetic dipole operators, as given by

$$\mathcal{L}_{\text{mag}} = iC_{VXX} \partial^{[\mu} V^{\nu]} (X_\mu^- X_\nu^+ - X_\mu^+ X_\nu^-), \quad (2.9)$$

where

$$C_{VXX} = g_D \sin \zeta \begin{cases} \cos \theta_w, & V_\mu = A_\mu, \\ (\sin \theta_w \cos \rho + \tan \zeta \sin \rho), & V_\mu = Z_\mu, \\ -(\sin \theta_w \sin \rho + \tan \zeta \cos \rho), & V_\mu = Z'_\mu. \end{cases} \quad (2.10)$$

The parameter ρ is defined as,

$$\rho \equiv \frac{1}{2} \arctan \left[\frac{m_Z^2 \sin \theta_w \sin(2\zeta)}{m_{\text{DM}}^2 \cos^2 \beta - m_Z^2 (\cos^2 \zeta - \sin^2 \theta_w \sin^2 \zeta)} \right]. \quad (2.11)$$

The above interactions play the key role to determine the phenomenology of the dark matter. For our analysis, we adopt a representative benchmark point with $\cos \beta = \sin \theta_t = 0.7$, where θ_t denotes the mixing angle between the neutral scalar states. The masses of the dark scalars are chosen to lie close to the DM mass scale, $m_{\Sigma_D^\pm} = m_{\Sigma_D^0} = m_{\Phi_D^0} = 1.2 m_{\text{DM}}$, but remain sufficiently heavy to kinematically forbid DM decay into Σ_D^\pm .

3 Freeze-out Relic Density

The relic density of DM, measured by *Planck* [35] to be $\Omega_{\text{DM,obs}} h^2 = 0.120 \pm 0.001$, is enforced in our analysis in the so-called *relic targets*, i.e. the contours in the parameter space

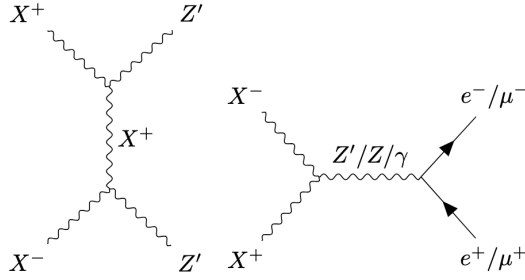


Figure 1: DM annihilation processes that set the relic abundance. The left diagram is dominant for small ζ , and the right for ζ close to 1.

that reproduce this observed value. The Boltzmann equation governing the cosmological DM number density, n_{DM} , is given by,

$$\dot{n}_{\text{DM}} + 3Hn_{\text{DM}} = -\frac{1}{2}\langle\sigma v_{\text{rel}}\rangle (n_{\text{DM}}^2 - n_{\text{DM,eq}}^2), \quad (3.1)$$

where H is the Hubble rate, and $\langle\sigma v_{\text{rel}}\rangle$ is the thermally averaged cross section of DM annihilation. We have implemented the model in **FeynRules**[36], computed thermally averaged cross sections and solve the Boltzmann equation under the freeze-out approximation [37] to calculate the relic density in terms of the model parameters, using an in-house developed Boltzmann solver in conjunction with **micrOMEGAs**[38]. For sub-GeV DM, annihilations into hadronic final states become important because, below the QCD confinement temperature, quarks no longer exist as free particles [39–41]. We therefore incorporate these hadronic channels when determining the relic targets, where they appear as resonances at DM masses satisfying $m_{\text{DM}} \simeq m_H/2$, with m_H the mass of the corresponding hadron.

In this model, DM may annihilate into either dark-sector or SM particles, with the dominant channels determined by the parameter regime. For small values of ζ , the model enters the *forbidden* regime [42], in which DM predominantly annihilates into dark-sector states. In this case, the process shown on the left of Fig. 1 controls the relic abundance. Additional channels, such as $X^+X^- \rightarrow Z'\Sigma_D^0$, $X^+X^- \rightarrow Z'\Phi_D^0$, and co-annihilations like $X^+\Sigma_D^- \rightarrow Z'\Phi_D^0$ and $X^+\Sigma_D^- \rightarrow Z'Z'$, are also included, though they contribute less than 10% to the total thermally averaged cross section $\langle\sigma v_{\text{rel}}\rangle$.

For larger values of ζ ($\sin\zeta \gtrsim 10^{-2}$), the model transitions to the *direct annihilation* regime, where DM primarily annihilates into SM final states. In this case, channels such as $X^+X^- \rightarrow e^+e^-$, $\mu^+\mu^-$, or hadronic states determine the relic density, with the co-annihilation process $X^+\Sigma_D^- \rightarrow \text{SM}$ providing a subdominant contribution.

3.1 Thermalization Condition

In the freeze-out scenario, the dark matter must remain in thermal equilibrium with the SM plasma prior to the decoupling [37]. Chemical equilibrium is maintained through annihilation (production) into (from) SM species, while kinetic equilibrium is achieved by elastic scattering with SM fermions and with the Z' . The corresponding interaction rate, $R \equiv n\langle\sigma v\rangle$, must exceed the Hubble expansion rate, H , at temperatures above freeze-out.

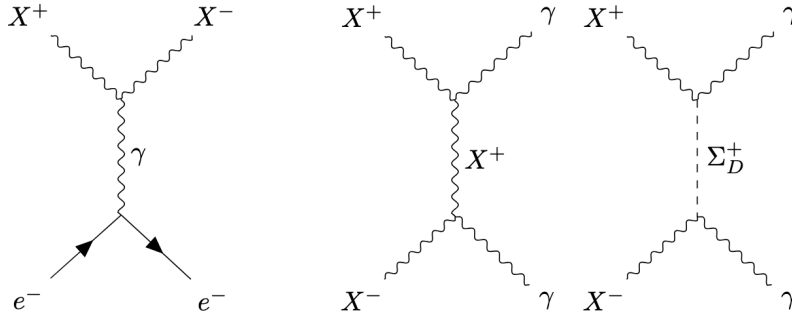


Figure 2: Direct and indirect detection processes. Left: DM-electron scattering that induces electronic excitations at direct detection experiments. Right: DM annihilation that injects energy into the CMB through velocity independent thermally averaged cross sections.

In this work, we explore values of $\sin\zeta$ spanning 10^{-10} to 1. Although this range includes extremely small portal couplings, the relatively large dark gauge coupling, $g_D \sim 10^{-4} - 10^{-2}$, ensures that the condition $R > H$ is always satisfied. The validity of the standard Boltzmann equation in Eq. (3.1) further requires DM to remain in kinetic equilibrium with the SM bath throughout freeze-out [43]; this criterion is also fulfilled across the parameter space considered here.

DM production through freeze-in [44, 45], rather than freeze-out, would occur for small values of g_D – which we leave as an interesting direction for future work.

4 Current Experimental Bounds

In this section, we provide a brief overview of the constraints on the model parameter space arising from existing terrestrial experiments and astrophysical observations.

4.1 Colliders

Dark photons decaying into SM final states, either promptly or long lived, after being produced in proton-proton or e^+e^- collisions are searched for at collider experiments. We consider the limits from the null results of the experiments LHCb [46], KLOE [47], BaBar [48], NA48/2 [49], and FASER [50], most relevant for the sub-GeV DM mass range.

4.2 Direct Detection

Direct detection experiments serve as the only way to directly measure and discover the DM present in our galaxy [51]². For WIMP scale DM, nuclear recoils are the conventional search strategy [53]. On the other hand, sub-GeV DM, due to its light mass, would not induce a sufficiently sized nuclear recoil to be observed. However, light DM can induce sizeable electronic excitations in the detector material from DM-electron scattering [5, 54].

²DM collider and indirect searches act as validation of potential direct detection discoveries [52], and as invaluable guiding tools for DM and other new physics beyond the SM.

DM-electron scattering proceeds through a t-channel diagram via a virtual photon, as drawn in Fig. 2. DM could also scatter via a virtual Z' or Z -boson, however we expect these contributions to be sub-leading since the momentum transfer squared is $\ll m_{Z'}, m_Z$.

From Eq. 2.9, we obtain the following non-relativistic amplitude for DM-electron scattering

$$i\mathcal{M} = -\frac{ieg_D \sin \zeta \cos \theta_w}{|\mathbf{q}|^2} \left[2 \frac{m_e}{m_{\text{DM}}} \delta^{s's} \mathbf{q} \cdot \mathbf{S}_{\text{DM}}^{\lambda'\lambda} \cdot \mathbf{q} + 2m_e \delta^{s's} \left(i\mathbf{q} \times \mathbf{v}^\perp \right) \cdot \mathbf{S}_{\text{DM}}^{\lambda'\lambda} \right. \\ \left. + 2|\mathbf{q}|^2 \mathbf{S}_e^{s's} \cdot \mathbf{S}_{\text{DM}}^{\lambda'\lambda} - 2 \left(\mathbf{q} \cdot \mathbf{S}_e^{s's} \right) \left(\mathbf{q} \cdot \mathbf{S}_{\text{DM}}^{\lambda'\lambda} \right) \right]. \quad (4.1)$$

Here, we adopt the notation of Ref. [55] where m_e is the electron mass, \mathbf{q} is the momentum transfer, \mathbf{v}^\perp is the transverse DM-electron relative velocity while $\mathbf{S}_e^{s's} = \xi^{\dagger s'} \mathbf{S}_e \xi^s$, $\mathbf{S}_e = \boldsymbol{\sigma}/2$ is the electron spin operator, $\boldsymbol{\sigma} = (\sigma_1, \sigma_2, \sigma_3)$ is a three-dimensional vector whose components are the three Pauli matrices, ξ^s , $s = 1, 2$, is a two-component spinor, $\mathbf{S}_{\text{DM}}^{\lambda'\lambda} = -ie'_{\lambda'} \times \mathbf{e}_\lambda$, $\mathbf{S}_{\text{DM}ij}^{\lambda'\lambda} = \frac{1}{2} \left(e_{\lambda i} e'_{\lambda' j} + e_{\lambda j} e'_{\lambda' i} \right)$ and $e_{\lambda i}$ is the i -th component of the λ -th DM polarization vector. From Eq. 4.1 and the null results reported by DAMIC-M [6] and PANDAX-4T [56], we derive 90% C.L. exclusion limits in the $(m_{\text{DM}}, \sin \zeta)$ plane. For DAMIC-M, we perform this calculation by requiring that the probability of observing a total number of signal plus background events smaller than or equal to the actually observed one in the one, two and three electron channels is at least 0.1. In doing so, we use the expected background reported in Tab. 1 of [6], and compute the rate of DM-induced electronic excitations in a silicon detector using the crystal response functions obtained in [57]. We assume the total detector efficiency given in [6] and an exposure of 1.257 kg-year. For PANDAX-4T, we impose that, in each of the eight ionization-charge bins considered in Ref. [56], the probability of observing a number of signal plus background events smaller than or equal to the actually observed one is at least 0.1. We extract the PANDAX-4T background model from Fig. 2 of Ref. [56] and compute the differential electron recoil energy rate using the xenon response functions derived in Ref. [55]. We then convert this into an ionization rate by applying the detector response model introduced in Ref. [58], the total detector efficiency reported in Fig. 1 of Ref. [56] and employing an exposure of 1.04 ton-year. For both experiments, we assume Poisson statistics for the observed number of counts.

4.3 Electroweak Precision Measurements

New physics which affect SM electroweak precision observables are constrained. Following [59] and [60], we check that precision measurements of the mass of the Z -boson and the coupling between the Z -boson and SM fermions do not exceed current values [61]. We find that these limits are not competitive with other limits considered in this study, but we leave a more comprehensive analysis of contributions from the extended scalar sector to future work. Furthermore, the invisible branching ratio of Higgs decays are excluded above

0.145 at 95% confidence level [62]. In this scenario, the process $H \rightarrow Z'Z'$ is found to be small, with a value of $\text{BR}_{H \rightarrow Z'Z'} \approx 4.6 \times 10^{-13}$ for $\sin \zeta = 0.1$ and $m_{\text{DM}} = 1 \text{ GeV}$.

4.4 Astrophysical and Cosmological Constraints

Energy Injection into the CMB

The annihilation of DM particles in the early universe injects energy into the CMB, which is constrained by current observations since it can change the recombination history, thus modifying the measured temperature and polarization power spectra [63]. For constraints from the CMB to be relevant, DM must annihilate with a cross section that is s-wave, such that it is not velocity suppressed³. In this model, DM annihilation into photons through the diagrams displayed in Fig. 2 are s-wave dominant, therefore the cross section is constant at low temperatures. We thus apply the 95% confidence level bound derived in [65] on the channel $\text{DM DM} \rightarrow \gamma\gamma$.

Big Bang Nucleosynthesis

Dark sector particles, especially of sub-GeV mass, thermally coupled to the SM and present during Big Bang Nucleosynthesis (BBN) can lead to alterations in the number of relativistic degrees of freedom, N_{eff} , affecting primordial abundances of light elements. The abundances of light elements are measured to a given precision, and any expected deviations from these observations lead to constraints on dark sector models [66–68]. A detailed consideration of constraints from BBN is beyond the scope of this work, however we include a conservative lower bound on the mass of the lightest dark species, Z' , to be $> 10 \text{ MeV}$. Thanks to the large dark coupling values, $g_D = 10^{-4}, 10^{-3}, 10^{-2}$, the Z' remains in thermal equilibrium with the SM thermal bath for all values of $\sin \zeta$ (down to $\sin \zeta = 10^{-10}$), therefore $m_{Z'} > 10 \text{ MeV}$ applies across the entire parameter space considered here.

Indirect Detection

Searches of DM annihilation products in astrophysical environments constrain the annihilation cross section of DM [69]. DM annihilation into SM fermion final states such as e^+e^- , $q\bar{q}$, proceed via p-wave (velocity) suppressed cross sections, leaving constraints through these channels weak. We thus only consider the velocity independent annihilation into $\gamma\gamma$ channel, drawn in Fig. 2 (right), where the dominant constraints come from CMB as discussed above.

Bullet Cluster

DM self-interactions are constrained by measurements of the colliding galaxy cluster, the Bullet Cluster [70, 71]. The cross section of DM self-interactions at non-relativistic energies, for all parameter values considered in this study, fall safely below the upper limit of $\sigma/m_{\text{DM}} < 1 \text{ cm}^2/\text{g}$ reported in [70].

³There does indeed exist bounds on p-wave annihilating DM [64], however they impose constraints that are not competitive with the other constraints we already consider in this work.

5 Sensitivity at Fixed-Target Experiments

In this section, we consider the most relevant experimental constraints and projections, including constraints from fixed target experiments, colliders, direct detection, electroweak precision measurements, BBN, and from energy injection into the CMB.

With the ongoing development of future fixed target experiments, such as LDMX [11, 72], and the current competitive limits coming from NA64 [31] and electron beam dump experiments [73], fixed target experiments are capable of extensively probing sub-GeV DM for numerous theoretical scenarios [8, 10, 13, 14, 45, 74]. Having a high energy beam of electrons (or protons in the case of SHiP [75] and other proton beam dumps) incident on a stationary target dense with nuclei, allows for a large number of potential DM events that can be detected through their missing energy or momentum (or through the direct scattering with a downstream detector in the case of proton beam dumps). However, for our scenario since $m_{Z'} < m_{\text{DM}}$, production of DM proceeds through off-shell processes and is thus suppressed relative to its on-shell counterpart. The on-shell production of visible species, in particular e^+e^- also occurs, acting as a complementary probe of this model. We consider the missing momentum search constraints from current NA64 null results and the sensitivity projections of the future experiment LDMX, in addition to the visible searches from past beam dump experiments E774 [76], E141 [77], Orsay [78], E137 [79], CHARM [80], KEK [81], and NuCal [82].

NA64’s 100 GeV electron beam incident on an active target composed of lead absorber layers, with 4.4×10^{11} electrons on target (EOT) so far, places competitive constraints on DM and dark sector particles that can be produced through these beam target interactions [31, 83]. We consider both visible and invisible production, where for the latter the production of DM through dark bremsstrahlung and through the decay of vector mesons are each capable of delivering missing energy signatures.

LDMX is a future missing-momentum experiment that will operate in two phases, where the second phase plans to have 10^{16} EOT with a beam energy of 8 GeV [72, 84]. With the ability to measure the transverse momentum, in addition to the energy, of the recoil electron after the interaction with the tungsten target, LDMX is subject to less background, projecting sensitivities reaching further than previous experiments in the on-shell case. In this study we explore the less studied and less sensitive off-shell / visible decay regime [12]. Similarly to NA64, LDMX will search for signatures from visible decays, dark bremsstrahlung, and invisible vector meson decay [85].

The two invisible production channels considered here for LDMX and NA64, dark bremsstrahlung (and dark Higgs-strahlung) and invisible vector meson decay, are plotted in Fig. 3 with LDMX experimental parameters and Phase II statistics. The analogous plot for current NA64 parameters and statistics is qualitatively similar, except with less events for both channels. Interestingly, the number of events from invisible vector meson decay exceeds dark bremsstrahlung by roughly five orders of magnitude for DM masses where mesons are kinematically allowed to decay to DM. Below, we discuss each channel, invisible and visible, in more detail.

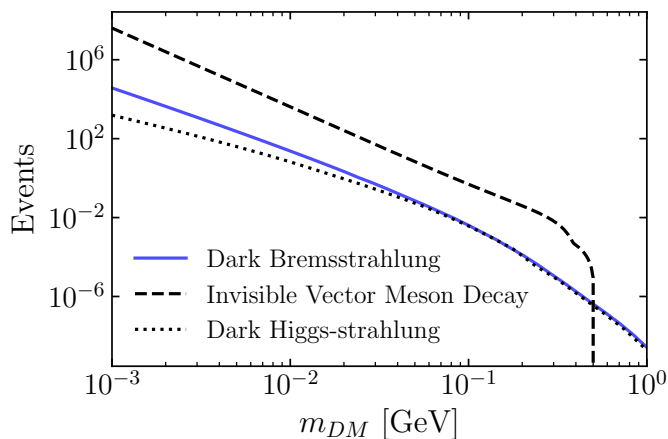


Figure 3: The number of DM events expected at LDMX Phase II, with a beam energy of 8 GeV and 10^{16} EOT, for two DM production channels: dark bremsstrahlung (in solid) and invisible vector meson decay (in dashed). The model parameters are set to: $\zeta = 10^{-3}$, $g_D = 0.01$, and the scalar masses are $m_{\Sigma_D^\pm} = m_{\Sigma_D^0} = m_{\Phi_D^0} = 1.2 m_{DM}$.

5.1 Dark Bremsstrahlung

Beam electrons incident on a target could produce dark sector particles in a process similar to ordinary bremsstrahlung. In the usual dark photon kinetic mixing scenario where $m_{A'} > 2m_{DM}$ [10], the dark photon is produced on-shell and later decays to DM, therefore the event rate is independent of the DM properties and is only dependent on the dark photon. In our scenario however, there is the off-shell production of DM through a virtual Z' or ordinary photon, since the mass hierarchy is reversed such that $m_{DM} > m_{Z'}$. Off-shell production of DM is suppressed compared to on-shell production [12], leading to less expected events. Dark bremsstrahlung processes that occur dominantly for our choice of model parameters, namely the emission of DM off the initial or final state electron, and dark Bethe-Heitler trident processes, are drawn in Fig. 4.

Dark bremsstrahlung diagrams involving the new scalars, Φ_D^0 , Σ_D^0 , and Σ_D^\pm , as intermediate states, become relevant as $\sin \beta$ approaches 0, however for the choice of parameters where $\cos \beta = 0.7$, these diagrams contribute negligibly to the production of dark states. Simulations of dark bremsstrahlung events are performed in **MadGraph** [86], with UFO files [87] generated by our **FeynRules** model file [36]. The DM and dark scalar vertices, in addition to the nucleus-photon vertex with form factor from [88]⁴, are included in our UFO files.

As evident by Fig. 3, dark bremsstrahlung events are much less than that of invisible vector meson decay, due to the off-shell nature of the dark brem.

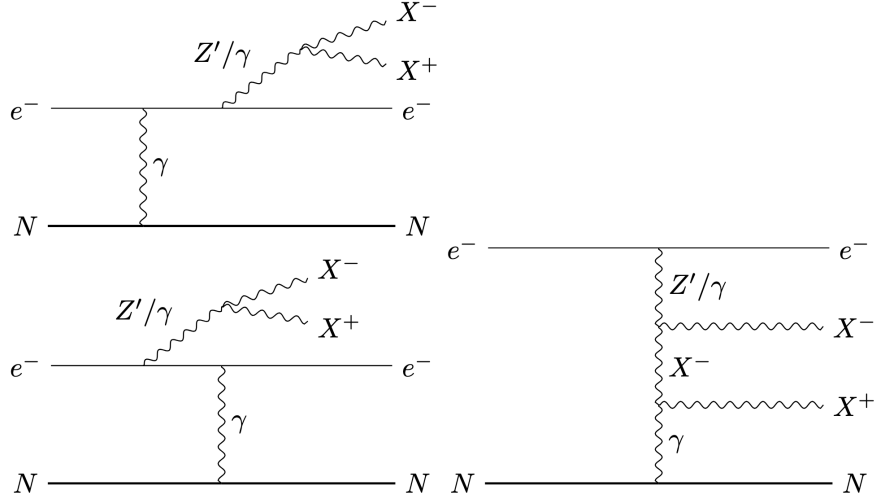


Figure 4: The dominant off-shell dark bremsstrahlung processes generating DM that occur at fixed target experiments, where N represents the target nucleus. Left: DM production diagrams off the initial or final state beam electron. Right: Bethe-Heitler trident diagrams for DM production.

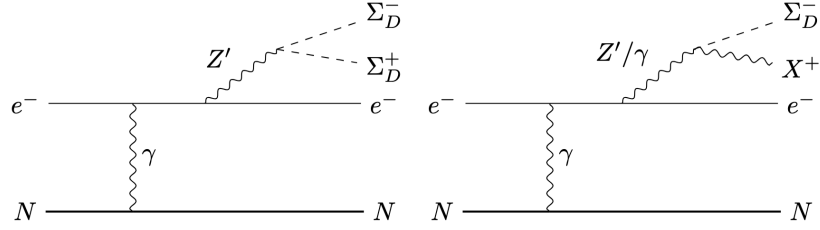


Figure 5: Examples of dark Higgs-strahlung processes providing additional missing energy/momentum signatures.

5.2 Dark Higgs-strahlung

Not only can the production of DM itself produce a missing momentum signature, but also the production of new scalars [89, 90], since similarly to DM, dark scalars would not interact in the detector. In our set up, the production of scalars $\Sigma_D^{\pm/0}, \Phi_D^0$ through the process $e^- N \rightarrow e^- N S$, where S is final states such as $\Sigma_D^{+(-)} X^{-(+)}$, $\Sigma_D^+ \Sigma_D^-$, and Σ_D^0 / Φ_D^0 , would look like a missing energy/momentum signature at an experiment like LDMX, similarly to a signature from DM production. The final states $\Sigma_D^{+(-)} X^{-(+)}$ make up the largest contribution of events. The processes with final states $\Phi_D^0 Z'$ and $\Sigma_D^0 Z'$ also occur, however there is only *missing* energy/momentum if the Z' decays visibly outside of the detector.

We draw the most prominent dark Higgs-strahlung diagrams resulting in missing en-

⁴The form factor from A18 and A19 of [88], which is used as an approximate representation of the effects from the atomic/nuclear structure, has a typo in Eq. A19: the second term should not be squared.

ergy/momentum signatures in Fig. 5. Trident style diagrams where the new scalars are produced from the virtual photon exchanged by the nucleus also exist, although we find their contribution to be sub-leading. As evident by Fig. 3, the dark Higgs-strahlung cross section is of similar magnitude to dark bremsstrahlung.

5.3 Invisible Vector Meson Decay

In addition to the dark bremsstrahlung process, DM can also be produced invisibly through vector meson decays generated in beam-target collisions – the so called *invisible vector meson decay* [85]. Bremsstrahlung photons are converted to vector mesons through exclusive photoproduction processes, which then decay to DM through a mediator that mixes with vector mesons. The three possible vector mediators in this model are the photon, Z boson, and Z' . The Z boson is heavy compared to the vector mesons, resulting in a much smaller cross section than those of the other two mediators. There is a larger cross section through the ordinary photon, however not as high as through the Z' – which has a mass less than the DM but similar order of magnitude. Therefore, we consider the process $V \rightarrow Z' \rightarrow X^+ X^-$, where V is a vector meson such as the ρ , ω , ϕ , or J/ψ , and the Z' is off-shell. Since the Z' couples to SM quarks through vector currents, the Z' mixes with the vector mesons with the form factors given in the fourth line of Table III of [85]. Following the methodology of [85], and adapting to this model, we compute the predicted number of DM events from invisible vector meson decays for the experiments NA64 [31] and LDMX [11, 72]. The number of events from the decay of a vector meson V is given by,

$$N_{\text{DM}} = \sum_V N_V Br(V \rightarrow X^+ X^-), \quad (5.1)$$

where N_V is the predicted number of vector mesons produced from beam target collisions and $Br(V \rightarrow X^+ X^-) \equiv \frac{\Gamma_{V \rightarrow X^+ X^-}}{\Gamma_V}$ where the decay rate to DM is written in Appendix A and Γ_V is measured experimentally and reported in PDG [91]. The sum runs over $V = \rho, \omega, \phi$ and in the case of NA64, additionally J/ψ since the beam energy of 100 GeV is sufficiently high. We use the corresponding values found in Table II of [85] for N_V , calculated using a combination of experimental measurements and theory. We take the currently reported EOT at NA64 to be 4.4×10^{11} , and thus scale-up the corresponding values in Table II of [85] to be $N_\rho = 1.1 \times 10^7$, $N_\omega = 7.9 \times 10^5$, $N_\phi = 7.0 \times 10^5$, and $N_{J/\psi} = 9.7 \times 10^3$. For LDMX, we take the corresponding values for Phase II reported in Table II of [85].

90% confidence level constraints and projections for invisible vector meson decays at NA64 and LDMX, respectively, for each specie of meson are plotted in Fig. 6 as a function of the model parameters. The reach of LDMX surpasses that of NA64 due to the increased statistics, providing a significant improvement to the sensitivity landscape from the data that will come from LDMX. Interestingly, since the $V \rightarrow X^+ X^-$ decay rate is proportional to $1/m_{\text{DM}}^4$, the sensitivity increases as m_{DM} decreases – resulting in much more sensitivity for lower masses compared to the on-shell dark photon studied in [85], which features a sensitivity that is independent of m_{DM} . Due to the inverse mass hierarchy, where $m_{\text{DM}} > m_{Z'}$, the sensitivity lacks the resonance that exists in the on-shell

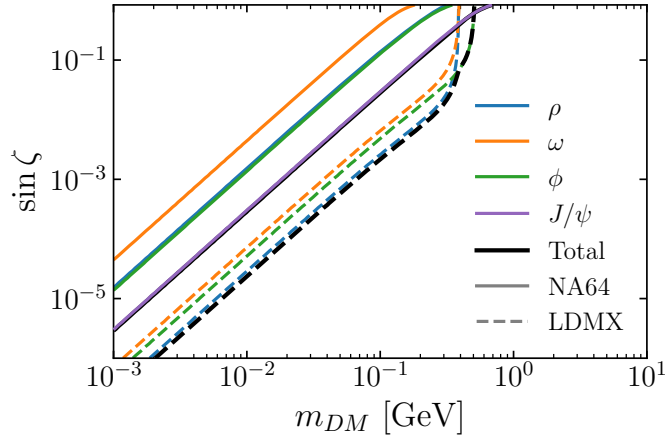


Figure 6: 90% confidence level constraints from current NA64 null results [31] (in solid) and projections for LDMX Phase II [11] (in dashed), from invisible vector meson decay. The contribution from each vector meson is plotted in colour, and the total in black. g_D is set to 10^{-2} .

dark photon case; since at $m_{Z'} \approx m_V$, the condition $m_V > 2m_{DM}$ for the decay to be allowed, would not hold.

As evident by Fig. 3, the sensitivity from inverse meson decays exceed that of dark bremsstrahlung.

5.4 Visible Searches

Finally, the Z' decays visibly to SM final states f^+f^- , the only decay channel kinematically allowed, and can be searched for as displaced visible energy depositions in the detectors [11, 12, 92, 93] or as missing energy/momentum if it decays outside of the detector. We consider displaced visible energy deposition limits from existing experiments NA64 [94], electron beam dump experiments E774, E141, Orsay, KEK, and E137 [73], proton beam dumps CHARM and NuCal [82, 95].

For LDMX Phase II projections, we compute limits from displaced visible events and also events from missing energy/momentum in which the Z' decays outside of the detector. The number of events from a visibly decaying Z' is [12],

$$N_{\text{vis}} = N_{Z'} (e^{-z_{\text{min}}/\gamma c\tau} - e^{-z_{\text{max}}/\gamma c\tau}), \quad (5.2)$$

where z_{min} and z_{max} are the distance to the beginning and end of the detector, respectively, γ is the Z' boost, and $c\tau$ ⁵ is the proper decay length of Z' .

For LDMX Phase II we take 10^{16} EOT, with $z_{\text{min}} = 43$ cm and $z_{\text{max}} = 315$ cm for the visible signature, and $z_{\text{min}} = 315$ cm and $z_{\text{max}} = \infty$ for the invisible signature. We use the approximate expression for the number of Z' 's produced in beam-target collisions as a

⁵We restore c for clarity when quoting decay lengths in physical units.

function of $m_{Z'}$ and couplings [12],

$$N_{Z'} \approx \frac{7}{10^{-5}} \left(\frac{4 \sin^2 \theta_w \sin \rho - \sin \rho + 3 \cos \rho \tan \zeta \sin \theta_w}{4 \cos \theta_w \sin \theta_w} \right)^2 \left(\frac{100 \text{ MeV}}{m_{Z'}} \right)^2. \quad (5.3)$$

6 Relic Targets, Constraints, and LDMX Projections

Fig. 7 presents the leading constraints on our model in the $\sin \zeta$ vs m_{DM} plane, for three benchmark values of g_D . Constraints from current experimental data are marked as shaded

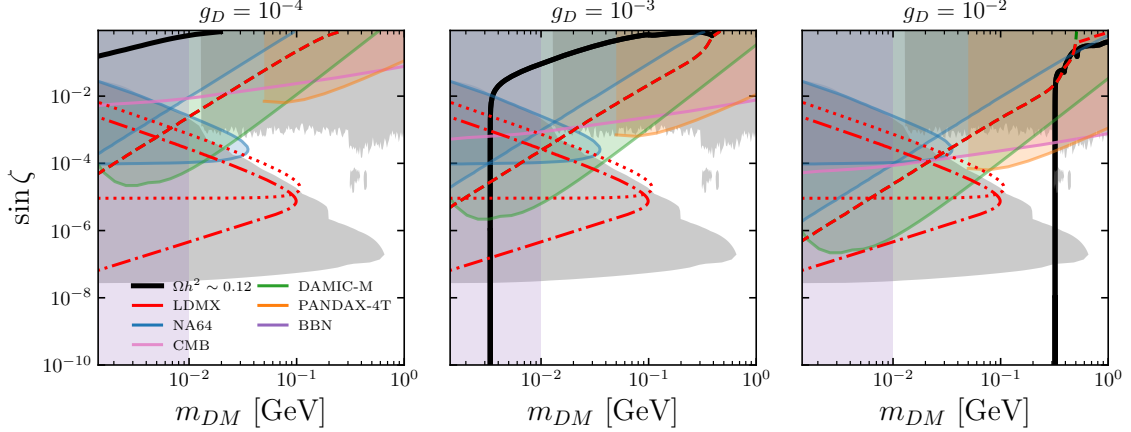


Figure 7: Summary of the most relevant constraints on this model in the $\sin \zeta$ vs m_{DM} parameter space, overlaid with the relic targets (curves reproducing the observed relic abundance consistent with Planck) [35] shown as thick solid lines. The three subplots differ by the value of the g_D parameter: with $g_D = 10^{-4}$ on the left, $g_D = 10^{-3}$ in the middle, and $g_D = 10^{-2}$ on the right. 90% confidence level projections for LDMX Phase II [11] are drawn in red: invisible vector meson decay is drawn in dashed, and visible decay of the $Z' \rightarrow e^+e^-$ outside of the detector in dash-dot and inside of the detector in dotted. 90% confidence levels for NA64 [31] from invisible vector meson decay and visible Z' decay [96] at current statistics are in blue. The pink curves indicate regions in which the parameters are constrained by CMB measurements [65] at 95% confidence level. Direct detection 90% confidence level constraints from DAMIC-M are plotted in green [6] and from PANDAX-4T in orange [97]. Grey regions are excluded at 95% confidence level by the beam dump experiments CHARM, E774, E141, Orsay, KEK, and E137 [73], and at 90% by NuCal [82], along with collider experiments LHCb [46], KLOE [47], BaBar [48], NA48/2 [49], and FASER [50] at 90%.

regions, while projected constraints from the up-coming LDMX are in dashed, dotted, and dash-dotted, corresponding to invisible vector meson decay, visible decays, and visible decays outside of the detector, respectively.

The relic targets in black vary depending on the *regime* defined by the parameter values and corresponding dominant DM annihilation processes in the early universe. The *forbidden* regime, as discussed in Section 3, occurs for values of $\sin \zeta \lesssim 0.01$. In this

regime, only dark sector processes (left diagram of Fig. 1) contribute to the relic abundance, therefore the relic target is independent of ζ . The cross section of $X^+X^- \rightarrow Z'Z'$ is inversely proportional to m_{DM} , thus increasing the coupling results in the relic target shifting to larger DM masses, explaining the shift to larger masses with increasing g_D . One can imagine how values of g_D in between or outside of the values considered would alter the relic targets. If $g_D = 0.1$, we are no longer in the sub-GeV DM regime, therefore we leave that investigation for future work. The *direct annihilation* regime occurs for $\sin \zeta \gtrsim 0.01$, where DM annihilation to SM final states sets the relic abundance. This regime is dependent on ζ , thus exhibits a sloped relic target with a kink associated with the onset of annihilations to $\mu^+\mu^-$, and resonances corresponding to hadronic final states.

Constraints from the null result of existing beam dump and collider experiments searching for visible signatures from dark sectors, indicated by grey shaded regions, provide large coverage over the parameter space. Interestingly, for both LDMX and NA64, the sensitivity from invisible meson decays surpasses that of dark bremsstrahlung (including dark Higgs-strahlung), as discussed in more detail in Section 5. Furthermore, direct detection from DAMIC-M, in green, provide even stronger constraints. Limits from the CMB extend the constrained parameter region for $g_D = 10^{-2}$, where they slightly outperform existing collider constraints. Although projections of LDMX Phase II (in red), for both visible and invisible searches, do not dramatically extend the sensitivity, it will however provide valuable validation of previous results, such as those from FASER. These results are not unexpected; being in the kinematic regime where the mediator cannot be produced on-shell leads to off-shell suppression of invisible final states, and the availability of visible search channels. Notice how all constraints that are dependent on the dark sector coupling, g_D , (direct detection, CMB, and invisible vector meson decays at fixed targets), become stronger compared to visible searches, as g_D becomes larger. These results highlight the complementarity between different types of DM searches – from cosmological, laboratory, and astrophysical, searches.

Evidently, $g_D \lesssim 10^{-3}$ is ruled out by BBN and current experimental search limits. This leaves $g_D \sim 10^{-2}$, for $\sin \zeta \lesssim 4 \times 10^{-8}$ down to arbitrarily small values, in addition to the gap in sensitivity around $\sin \zeta \sim 10^{-5}$ for $m_{\text{DM}} \gtrsim 100$ MeV, still viable.

7 Conclusion

We extend our previous work [13] on light spin-1 DM at LDMX (and other relevant fixed target experiments) to the case with a reversed mass hierarchy, $m_{Z'} < 2m_{\text{DM}}$, which alters the phenomenology and thus provides new search opportunities at LDMX and other relevant experiments. We demonstrate a viable light spin-1 DM model which includes an extension to the SM gauge symmetry by a new $SU(2)$, a Z' mediator, two new scalars, and a higher dimensional portal interaction between the dark sector and SM. The extended scalar sector that we outline, is capable of explaining the mass generation of DM and the Z' , and also plays a role phenomenologically at fixed target experiments.

The relic abundance of DM is computed, where the DM undergoes freeze-out in the early universe. The annihilation processes dominantly responsible for setting the relic abun-

dance range from dark sector only processes in the forbidden regime, to direct annihilation into SM fermions at larger portal couplings.

Our primary focus is on processes giving rise to signatures at fixed target experiments LDMX and NA64, under this reversed mass hierarchy scenario. While on-shell invisible mediator production is kinematically forbidden, we consider: off-shell dark bremsstrahlung into DM final states, dark Higgs-strahlung into dark scalar final states, invisible vector meson decays, and visible searches through decays of the Z' mediator to SM. We compute complementary constraints from direct detection, CMB, collider searches, and BBN. The dominant constraints come from DAMIC-M and PANDAX-4T via DM-electron scattering, collider and beam dump visible searches, and the CMB. A region of the parameter space remains unconstrained at $g_D \sim 10^{-2}$, $m_{\text{DM}} \gtrsim 100$ GeV.

Acknowledgments

A.B. would like to thank the Chalmers University of Technology, Göteborg, Sweden for support during the initial stages of this work, and acknowledges support from the Department of Atomic Energy, Govt. of India. R.C. acknowledges support from an individual research grant from the Swedish Research Council (Dnr. 2022-04299). R.C. and T.G. have also been funded by the Knut and Alice Wallenberg Foundation, and performed their research within the “Light Dark Matter” project (Dnr. KAW 2019.0080).

A Invisible Vector Meson Decay Rate

The decay rate of a vector meson, V , into vector DM through the Z' is,

$$\begin{aligned} \Gamma_{V \rightarrow Z' \rightarrow X^+ X^-} = & \frac{f_V^2 g_V^2 g_D^2 (m_V^2 - 4m_{\text{DM}}^2)^{3/2}}{192\pi \cos^2 \zeta m_{\text{DM}}^4 ((m_{Z'}^2 - m_V^2)^2 + \Gamma_{Z'}^2 m_{Z'}^2)} \\ & \times \left[\cos^2 \rho \left(4m_{\text{DM}}^2 m_V^2 (\sin^4 \zeta - 5 \sin^2 \zeta + 5) + m_V^4 (\sin^2 \zeta - 1)^2 + 12m_{\text{DM}}^4 \right) \right. \\ & + 2m_V^2 \cos \rho \sin \rho \sin \zeta \cos \zeta \sin \theta_w \left(2m_{\text{DM}}^2 (2 \sin^2 \zeta - 5) + m_V^2 (\sin^2 \zeta - 1) \right) \\ & \left. + m_V^2 \sin^2 \rho \sin^2 \zeta \cos^2 \zeta \sin^2 \theta_w \left(4m_{\text{DM}}^2 + m_V^2 \right) \right], \end{aligned} \quad (\text{A.1})$$

where $g_V = \frac{e(4 \sin^2 \theta \sin \rho - \sin \rho + 3 \cos \rho \tan \zeta \sin \theta_w)}{4 \cos \theta_w \sin \theta_w}$, where f_V is the form factor for the coupling of mesons with a vector current taken from Table III of [85] which is derived from [98].

References

- [1] C. Balazs, T. Bringmann, F. Kahlhoefer and M. White, *A Primer on Dark Matter*, [2411.05062](#).

- [2] G. Arcadi, M. Dutra, P. Ghosh, M. Lindner, Y. Mambrini, M. Pierre et al., *The waning of the WIMP? A review of models, searches, and constraints*, *Eur. Phys. J. C* **78** (2018) 203 [[1703.07364](#)].
- [3] G. Steigman and M.S. Turner, *Cosmological Constraints on the Properties of Weakly Interacting Massive Particles*, *Nucl. Phys. B* **253** (1985) 375.
- [4] B.W. Lee and S. Weinberg, *Cosmological Lower Bound on Heavy Neutrino Masses*, *Phys. Rev. Lett.* **39** (1977) 165.
- [5] A. Mitridate, T. Trickle, Z. Zhang and K.M. Zurek, *Snowmass white paper: Light dark matter direct detection at the interface with condensed matter physics*, *Phys. Dark Univ.* **40** (2023) 101221 [[2203.07492](#)].
- [6] DAMIC-M collaboration, *Probing Benchmark Models of Hidden-Sector Dark Matter with DAMIC-M*, *Phys. Rev. Lett.* **135** (2025) 071002 [[2503.14617](#)].
- [7] E. Izaguirre, G. Krnjaic, P. Schuster and N. Toro, *Analyzing the Discovery Potential for Light Dark Matter*, *Phys. Rev. Lett.* **115** (2015) 251301 [[1505.00011](#)].
- [8] G. Krnjaic et al., *A Snowmass Whitepaper: Dark Matter Production at Intensity-Frontier Experiments*, [2207.00597](#).
- [9] S. Balan et al., *Resonant or asymmetric: the status of sub-GeV dark matter*, *JCAP* **01** (2025) 053 [[2405.17548](#)].
- [10] A. Berlin, P. deNiverville, A. Ritz, P. Schuster and N. Toro, *Sub-GeV dark matter production at fixed-target experiments*, *Phys. Rev. D* **102** (2020) 095011 [[2003.03379](#)].
- [11] LDMX collaboration, *LDMX – The Light Dark Matter EXperiment*, [2508.11833](#).
- [12] A. Berlin, N. Blinov, G. Krnjaic, P. Schuster and N. Toro, *Dark Matter, Millicharges, Axion and Scalar Particles, Gauge Bosons, and Other New Physics with LDMX*, *Phys. Rev. D* **99** (2019) 075001 [[1807.01730](#)].
- [13] R. Catena and T.R. Gray, *Spin-1 thermal targets for dark matter searches at beam dump and fixed target experiments*, *JCAP* **11** (2023) 058 [[2307.02207](#)].
- [14] R. Catena, T.R. Gray and T. Jerkvall, *Production of Dark Photons through Higher Electromagnetic Moments at LDMX: Simulations and Model Discrimination*, [2502.13635](#).
- [15] T. Hambye, *Hidden vector dark matter*, *JHEP* **01** (2009) 028 [[0811.0172](#)].
- [16] S.-M. Choi, H.M. Lee, Y. Mambrini and M. Pierre, *Vector SIMP dark matter with approximate custodial symmetry*, *JHEP* **07** (2019) 049 [[1904.04109](#)].
- [17] Z. Hu, C. Cai, Y.-L. Tang, Z.-H. Yu and H.-H. Zhang, *Vector dark matter from split $SU(2)$ gauge bosons*, *JHEP* **07** (2021) 089 [[2103.00220](#)].
- [18] T. Nomura, H. Okada and S. Yun, *Vector dark matter from a gauged $SU(2)$ symmetry*, *JHEP* **06** (2021) 122 [[2012.11377](#)].
- [19] T. Nomura and H. Okada, *Radiative neutrino mass model in dark non-Abelian gauge symmetry*, *Phys. Rev. D* **105** (2022) 075010 [[2106.10451](#)].
- [20] T. Nomura and H. Okada, *Radiative interactions between new non-Abelian gauge sector and the standard model*, *Phys. Lett. B* **821** (2021) 136630 [[2104.01871](#)].
- [21] R. Ramos, V.Q. Tran and T.-C. Yuan, *A Sub-GeV Low Mass Hidden Dark Sector of $SU(2)_H \times U(1)_X$* , *JHEP* **11** (2021) 112 [[2109.03185](#)].

- [22] T. Abe, M. Fujiwara, J. Hisano and K. Matsushita, *A model of electroweakly interacting non-abelian vector dark matter*, *JHEP* **07** (2020) 136 [[2004.00884](#)].
- [23] X. Chu, J. Hisano, A. Ibarra, J.-L. Kuo and J. Pradler, *Multipole vector dark matter below the GeV scale*, *Phys. Rev. D* **108** (2023) 015029 [[2303.13643](#)].
- [24] G. Krnjaic and T. Trickle, *Absorption of vector dark matter beyond kinetic mixing*, *Phys. Rev. D* **108** (2023) 015024 [[2303.11344](#)].
- [25] R. Catena, K. Fridell and M.B. Krauss, *Non-relativistic Effective Interactions of Spin 1 Dark Matter*, *JHEP* **08** (2019) 030 [[1907.02910](#)].
- [26] R. Catena, K. Fridell and V. Zema, *Direct detection of fermionic and vector dark matter with polarised targets*, *JCAP* **11** (2018) 018 [[1810.01515](#)].
- [27] N. Benincasa, L. Delle Rose, L. Panizzi, M. Razzaq and S. Urzetta, *Phase transitions and gravitational waves in a non-abelian vector dark matter scenario*, [2506.22248](#).
- [28] A. Belyaev, M. Bertenstam, J. Gonçalves, A.P. Morais, R. Pasechnik and N. Thongyoi, *Gravitational Waves from Dark Gauge Sectors*, [2508.04912](#).
- [29] G. Krnjaic, D. Rocha and A. Sokolenko, *Freezing in vector dark matter through magnetic dipole interactions*, *Phys. Rev. D* **108** (2023) 035047 [[2210.06487](#)].
- [30] A.L. Foguel, R.Z. Funchal and M. Frigerio, *Vector dark matter with non-abelian kinetic mixing*, [2510.26765](#).
- [31] NA64 collaboration, *Searching for Light Dark Matter and Dark Sectors with the NA64 experiment at the CERN SPS*, [2505.14291](#).
- [32] T. Biekötter and M. Pierre, *Higgs-boson visible and invisible constraints on hidden sectors*, *Eur. Phys. J. C* **82** (2022) 1026 [[2208.05505](#)].
- [33] ATLAS collaboration, *Combination of Searches for Higgs Boson Pair Production in pp Collisions at $s=13$ TeV with the ATLAS Detector*, *Phys. Rev. Lett.* **133** (2024) 101801 [[2406.09971](#)].
- [34] CMS collaboration, *Constraints on the Higgs boson self-coupling from the combination of single and double Higgs boson production in proton-proton collisions at $s=13$ TeV*, *Phys. Lett. B* **861** (2025) 139210 [[2407.13554](#)].
- [35] PLANCK collaboration, *Planck 2018 results. VI. Cosmological parameters*, *Astron. Astrophys.* **641** (2020) A6 [[1807.06209](#)].
- [36] A. Alloul, N.D. Christensen, C. Degrande, C. Duhr and B. Fuks, *FeynRules 2.0 - A complete toolbox for tree-level phenomenology*, *Comput. Phys. Commun.* **185** (2014) 2250 [[1310.1921](#)].
- [37] P. Gondolo and G. Gelmini, *Cosmic abundances of stable particles: Improved analysis*, *Nucl. Phys. B* **360** (1991) 145.
- [38] G. Belanger, F. Boudjema, A. Pukhov and A. Semenov, *micrOMEGAs_3: A program for calculating dark matter observables*, *Comput. Phys. Commun.* **185** (2014) 960 [[1305.0237](#)].
- [39] E. Izaguirre, G. Krnjaic and B. Shuve, *Discovering Inelastic Thermal-Relic Dark Matter at Colliders*, *Phys. Rev. D* **93** (2016) 063523 [[1508.03050](#)].
- [40] P. Ilten, Y. Soreq, M. Williams and W. Xue, *Serendipity in dark photon searches*, *JHEP* **06** (2018) 004 [[1801.04847](#)].

- [41] Z. et al. (Particle Data Group), *Review of Particle Physics*, *Progress of Theoretical and Experimental Physics* **2020** (2020) [<https://academic.oup.com/ptep/article-pdf/2020/8/083C01/34673722/ptaa104.pdf>].
- [42] R.T. D’Agnolo and J.T. Ruderman, *Light Dark Matter from Forbidden Channels*, *Phys. Rev. Lett.* **115** (2015) 061301 [[1505.07107](#)].
- [43] T. Binder, T. Bringmann, M. Gustafsson and A. Hryczuk, *Early kinetic decoupling of dark matter: when the standard way of calculating the thermal relic density fails*, *Phys. Rev. D* **96** (2017) 115010 [[1706.07433](#)].
- [44] L.J. Hall, K. Jedamzik, J. March-Russell and S.M. West, *Freeze-In Production of FIMP Dark Matter*, *JHEP* **03** (2010) 080 [[0911.1120](#)].
- [45] C. Cosme, M. Dutra, S. Godfrey and T.R. Gray, *Testing freeze-in with axial and vector Z' bosons*, *JHEP* **09** (2021) 056 [[2104.13937](#)].
- [46] LHCb collaboration, *Search for $A' \rightarrow \mu^+ \mu^-$ Decays*, *Phys. Rev. Lett.* **124** (2020) 041801 [[1910.06926](#)].
- [47] KLOE-2 collaboration, *Combined limit on the production of a light gauge boson decaying into $\mu^+ \mu^-$ and $\pi^+ \pi^-$* , *Phys. Lett. B* **784** (2018) 336 [[1807.02691](#)].
- [48] BABAR collaboration, *Search for a Dark Photon in $e^+ e^-$ Collisions at BaBar*, *Phys. Rev. Lett.* **113** (2014) 201801 [[1406.2980](#)].
- [49] NA48/2 collaboration, *Search for the dark photon in π^0 decays*, *Phys. Lett. B* **746** (2015) 178 [[1504.00607](#)].
- [50] FASER collaboration, *Search for dark photons with the FASER detector at the LHC*, *Phys. Lett. B* **848** (2024) 138378 [[2308.05587](#)].
- [51] M. Schumann, *Direct Detection of WIMP Dark Matter: Concepts and Status*, *J. Phys. G* **46** (2019) 103003 [[1903.03026](#)].
- [52] R. Catena, T.R. Gray and A. Lund, *On the dark matter origin of an LDMX signal*, [2411.10216](#).
- [53] J. Billard et al., *Direct detection of dark matter—APPEC committee report**, *Rept. Prog. Phys.* **85** (2022) 056201 [[2104.07634](#)].
- [54] R. Catena and N.A. Spaldin, *Linear response theory for light dark matter-electron scattering in materials*, *Phys. Rev. Res.* **6** (2024) 033230 [[2402.06817](#)].
- [55] R. Catena, T. Emken, N.A. Spaldin and W. Tarantino, *Atomic responses to general dark matter-electron interactions*, *Phys. Rev. Res.* **2** (2020) 033195 [[1912.08204](#)].
- [56] M. Zhang et al., *Search for Light Dark Matter with 259-day data in PandaX-4T*, [2507.11930](#).
- [57] R. Catena, T. Emken, M. Matas, N.A. Spaldin and E. Urdshals, *Crystal responses to general dark matter-electron interactions*, *Phys. Rev. Res.* **3** (2021) 033149 [[2105.02233](#)].
- [58] R. Essig, A. Manalaysay, J. Mardon, P. Sorensen and T. Volansky, *First Direct Detection Limits on sub-GeV Dark Matter from XENON10*, *Phys. Rev. Lett.* **109** (2012) 021301 [[1206.2644](#)].
- [59] C.P. Burgess, S. Godfrey, H. Konig, D. London and I. Maksymyk, *Model independent global constraints on new physics*, *Phys. Rev. D* **49** (1994) 6115 [[hep-ph/9312291](#)].

- [60] D. Alonso-González, D. Cerdéno, P. Foldenauer and J.M. No, *GeV-scale thermal dark matter from dark photons: tightly constrained, yet allowed*, [2507.11376](#).
- [61] PARTICLE DATA GROUP collaboration, *Review of particle physics*, *Phys. Rev. D* **110** (2024) 030001.
- [62] ATLAS collaboration, *Search for invisible Higgs-boson decays in events with vector-boson fusion signatures using 139 fb^{-1} of proton-proton data recorded by the ATLAS experiment*, *JHEP* **08** (2022) 104 [[2202.07953](#)].
- [63] PLANCK collaboration, *Planck 2015 results. XIII. Cosmological parameters*, *Astron. Astrophys.* **594** (2016) A13 [[1502.01589](#)].
- [64] H. Liu, T.R. Slatyer and J. Zavala, *Contributions to cosmic reionization from dark matter annihilation and decay*, *Phys. Rev. D* **94** (2016) 063507 [[1604.02457](#)].
- [65] T.R. Slatyer, *Indirect dark matter signatures in the cosmic dark ages. I. Generalizing the bound on s-wave dark matter annihilation from Planck results*, *Phys. Rev. D* **93** (2016) 023527 [[1506.03811](#)].
- [66] C. Giovanetti, M. Lisanti, H. Liu and J.T. Ruderman, *Joint Cosmic Microwave Background and Big Bang Nucleosynthesis Constraints on Light Dark Sectors with Dark Radiation*, *Phys. Rev. Lett.* **129** (2022) 021302 [[2109.03246](#)].
- [67] N. Sabti, J. Alvey, M. Escudero, M. Fairbairn and D. Blas, *Refined Bounds on MeV-scale Thermal Dark Sectors from BBN and the CMB*, *JCAP* **01** (2020) 004 [[1910.01649](#)].
- [68] P.F. Depta, M. Hufnagel, K. Schmidt-Hoberg and S. Wild, *BBN constraints on the annihilation of MeV-scale dark matter*, *JCAP* **04** (2019) 029 [[1901.06944](#)].
- [69] M. Cirelli, A. Kar and H. Shaikh, *Indirect searches for realistic sub-GeV Dark Matter models*, [2508.03819](#).
- [70] M. Markevitch, A.H. Gonzalez, D. Clowe, A. Vikhlinin, L. David, W. Forman et al., *Direct constraints on the dark matter self-interaction cross-section from the merging galaxy cluster 1E0657-56*, *Astrophys. J.* **606** (2004) 819 [[astro-ph/0309303](#)].
- [71] D. Wittman, N. Golovich and W.A. Dawson, *The Mismeasure of Mergers: Revised Limits on Self-interacting Dark Matter in Merging Galaxy Clusters*, *Astrophys. J.* **869** (2018) 104 [[1701.05877](#)].
- [72] LDMX collaboration, *Light Dark Matter eXperiment (LDMX)*, [1808.05219](#).
- [73] S. Andreas, C. Niebuhr and A. Ringwald, *New Limits on Hidden Photons from Past Electron Beam Dumps*, *Phys. Rev. D* **86** (2012) 095019 [[1209.6083](#)].
- [74] S. Gori et al., *Dark Sector Physics at High-Intensity Experiments*, [2209.04671](#).
- [75] SHiP collaboration, *Sensitivity of the SHiP experiment to light dark matter*, *JHEP* **04** (2021) 199 [[2010.11057](#)].
- [76] A. Bross, M. Crisler, S.H. Pordes, J. Volk, S. Errede and J. Wrbanek, *A Search for Shortlived Particles Produced in an Electron Beam Dump*, *Phys. Rev. Lett.* **67** (1991) 2942.
- [77] E.M. Riordan et al., *A Search for Short Lived Axions in an Electron Beam Dump Experiment*, *Phys. Rev. Lett.* **59** (1987) 755.
- [78] M. Davier and H. Nguyen Ngoc, *An Unambiguous Search for a Light Higgs Boson*, *Phys. Lett. B* **229** (1989) 150.

- [79] J.D. Bjorken, S. Ecklund, W.R. Nelson, A. Abashian, C. Church, B. Lu et al., *Search for Neutral Metastable Penetrating Particles Produced in the SLAC Beam Dump*, *Phys. Rev. D* **38** (1988) 3375.
- [80] S.N. Gninenko, *Constraints on sub-GeV hidden sector gauge bosons from a search for heavy neutrino decays*, *Phys. Lett. B* **713** (2012) 244 [[1204.3583](#)].
- [81] A. Konaka et al., *Search for Neutral Particles in Electron Beam Dump Experiment*, *Phys. Rev. Lett.* **57** (1986) 659.
- [82] Y.-D. Tsai, P. deNiverville and M.X. Liu, *Dark Photon and Muon $g - 2$ Inspired Inelastic Dark Matter Models at the High-Energy Intensity Frontier*, *Phys. Rev. Lett.* **126** (2021) 181801 [[1908.07525](#)].
- [83] NA64 collaboration, *Search for Light Dark Matter with NA64 at CERN*, *Phys. Rev. Lett.* **131** (2023) 161801 [[2307.02404](#)].
- [84] LDMX collaboration, *Photon-rejection power of the Light Dark Matter eXperiment in an 8 GeV beam*, *JHEP* **12** (2023) 092 [[2308.15173](#)].
- [85] P. Schuster, N. Toro and K. Zhou, *Probing invisible vector meson decays with the NA64 and LDMX experiments*, *Phys. Rev. D* **105** (2022) 035036 [[2112.02104](#)].
- [86] J. Alwall, R. Frederix, S. Frixione, V. Hirschi, F. Maltoni, O. Mattelaer et al., *The automated computation of tree-level and next-to-leading order differential cross sections, and their matching to parton shower simulations*, *JHEP* **07** (2014) 079 [[1405.0301](#)].
- [87] C. Degrande, C. Duhr, B. Fuks, D. Grellscheid, O. Mattelaer and T. Reiter, *UFO - The Universal FeynRules Output*, *Comput. Phys. Commun.* **183** (2012) 1201 [[1108.2040](#)].
- [88] J.D. Bjorken, R. Essig, P. Schuster and N. Toro, *New Fixed-Target Experiments to Search for Dark Gauge Forces*, *Phys. Rev. D* **80** (2009) 075018 [[0906.0580](#)].
- [89] F. Acanfora and F. Kahlhoefer, *Dark Higgs-strahlung at Belle II: A distinctive dark sector signature with displaced vertices and missing energy*, [2508.09247](#).
- [90] M. Duerr, A. Grohsjean, F. Kahlhoefer, B. Penning, K. Schmidt-Hoberg and C. Schwanenberger, *Hunting the dark Higgs*, *JHEP* **04** (2017) 143 [[1701.08780](#)].
- [91] PARTICLE DATA GROUP collaboration, *Review of Particle Physics*, *Phys. Rev. D* **98** (2018) 030001.
- [92] S. Andreas et al., *Proposal for an Experiment to Search for Light Dark Matter at the SPS*, [1312.3309](#).
- [93] S.N. Gninenko, *Search for MeV dark photons in a light-shining-through-walls experiment at CERN*, *Phys. Rev. D* **89** (2014) 075008 [[1308.6521](#)].
- [94] NA64 collaboration, *Improved limits on a hypothetical $X(16.7)$ boson and a dark photon decaying into e^+e^- pairs*, *Phys. Rev. D* **101** (2020) 071101 [[1912.11389](#)].
- [95] J. Blumlein and J. Brunner, *New Exclusion Limits for Dark Gauge Forces from Beam-Dump Data*, *Phys. Lett. B* **701** (2011) 155 [[1104.2747](#)].
- [96] NA64 collaboration, *Search for a Hypothetical 16.7 MeV Gauge Boson and Dark Photons in the NA64 Experiment at CERN*, *Phys. Rev. Lett.* **120** (2018) 231802 [[1803.07748](#)].
- [97] PANDAX collaboration, *Dark Matter Search Results from 1.54 Tonne-Year Exposure of PandaX-4T*, *Phys. Rev. Lett.* **134** (2025) 011805 [[2408.00664](#)].

- [98] A. Bharucha, D.M. Straub and R. Zwicky, $B \rightarrow V \ell^+ \ell^-$ in the Standard Model from light-cone sum rules, *JHEP* **08** (2016) 098 [[1503.05534](#)].